Failure modes of bonded wrapped composite joints for steel circular hollow sections in ultimate load experiments

He, Pei; Pavlovic, Marko

DOI
10.1016/j.engstruct.2021.113799

Publication date
2022

Document Version
Final published version

Published in
Engineering Structures

Engineering Structures 254 (2022) 113799

Contents lists available at ScienceDirect

Engineering Structures

journal homepage: www.elsevier.com/locate/engstruct

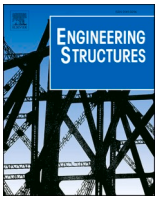

Failure modes of bonded wrapped composite joints for steel circular hollow sections in ultimate load experiments

Pei He, Marko Pavlovic *

Faculty of Civil Engineering and Geosciences, Delft University of Technology, Netherlands

ARTICLE INFO

Keywords:
CHS
Wrapped composite joints
Bonding
GFRP
Welded joints
Static behavior
Failure mechanism
3D DIC

ABSTRACT

The concept of an innovative bonded joining technology where welding is not required is presented as an alternative to traditional welded connection for steel circular hollow section (CHS). Wrapped composite joints have potential to greatly improve fatigue endurance when applied in multi-membered truss structures, e.g. offshore jackets for wind turbines. This paper focuses on characterization of resistance and understanding of failure modes of wrapped composite joints in static experiments, as the prerequisite for harvesting its potential for high fatigue endurance. Wrapped composite joints at two scales and with two different angles of X-joint geometry are made with GFRP composite material wrapped around steel sections without welding, and tested in 3 monotonic loading cases, tensile, compression and in-plane bending, until failure. Counterpart welded joints are tested at the smaller scale for stiffness, elastic limit and ultimate load comparisons. Two general failure modes of wrapped composite joints, debonding and fracture of the composite material are identified and quantified by surface strain measurements through 3D digital image correlation (DIC) technique. Testing results indicate that wrapped composite joints have 30% to 56% larger stiffness and 3% to 68% larger ultimate load compared to welded counterparts. Debonding and final pull-out of steel brace member from the composite wrap is predominant failure mode in tensile experiments at both scales while cracking of the composite material is the governing failure mode in the bending experiment. In tensile, compressive and bending experiments failure load of wrapped composite joints exceeds the yield resistance of the steel CHS indicating opportunity to optimize the composite wrapping thickness and length.

1. Introduction

Circular Hollow Sections (CHS) have been extensively used in engineering structures, as shown in Fig. 1, due to its high mechanical/cost efficiency, aesthetic, and good durability [1]. However, when applied in off-shore jacket structure and steel bridges where long-term cyclic loading is prevalent, CHS joints, traditionally formed by welded connecting brace (diagonal) to the chord member, encounter severe fatigue problem [2–4]. The low fatigue endurance of welded CHS joints results from high and complex stress conditions as consequence of local bending of the thin-walled CHS sections and ovalization in the welded intersection areas. Further reasons for stress concentrations are discontinuities at local notches, e.g. at the toes of butt welds and at the toes and roots of fillet welds, where sharp changes of direction occur [5]; and geometric peak stresses due to the non-uniform stiffness distribution at the perimeter of the connection [1]. In addition, welding results in residual stresses in the heat affected zone and embrittlement of the steel material.

Fibre polymer composites (a.k.a. Fibre Reinforced Polymer – FRP), further referred to as composites, have excellent corrosion and fatigue resistance in addition to high strength-to-weight ratio. With tailorable material properties by choosing the type of fibre (glass or carbon, etc.) and resin and ease of providing complex shapes through molding and lamination composites have potential in application with steel hollow sections, as hybrid joints, in fatigue-dominated loading conditions. Increasing interest of research has been seen in last two decades towards strengthening of existing welded circular hollow section (CHS) joints with composite material. The main focus is on steel butt joints [6–7], steel T joints [8–9], steel Y joints [10] and steel gap K joints [11–12]. The conclusion of all previous research is that retrofitting steel CHS joints by composites can enhance loading capacity of those joints substantially, and unfavorable failure modes, i.e., chord ovalization and punching shear, are efficiently mitigated.

Despite improved static behavior of composite-strengthened CHS

* Corresponding author.
E-mail address: M.Pavlovic@tudelft.nl (M. Pavlovic).

https://doi.org/10.1016/j.engstruct.2021.113799
Received 23 August 2021; Received in revised form 10 December 2021; Accepted 23 December 2021
Available online 16 January 2022

joints, main load is carried through welded connection, which remains to be a source of stress concentration and brittle failure under fatigue load. To fully unlock application potential of CHS restricted by current welding technology in many cases, the concept of innovative wrapped composite joints is proposed by TU Delft [13] as an alternative to traditional welded joints, as shown in Fig. 2. CHS brace members (diagonals) and the chord member in this case are bonded together by composite wrap which can be shaped in an optimal manner to decrease stress concentration at the bonded interface. Initial tensile static tests presented in TU Delft [14–16] prove their improved initial stiffness and equivalent load resistance compared to welded joints. The prerequisite for harvesting the potential for high fatigue endurance of wrapped composite joints applied in structures is good performance in terms of static resistance and understanding of failure modes.

Major problem in characterizing static behavior of wrapped composite joints is the complexity resulting from the variety of possible failure modes in these joints. Unlike composite-to-concrete bonded joints, in which failure is determined by fracture of the concrete substrate, a number of failure modes could govern the strength of composite-to-steel bonded joints [17]: 1) Adhesion failure between steel and the adhesive; 2) Cohesion failure, which is a failure of the adhesive layer; 3) Adhesion failure between composite and the adhesive; 4) Delamination of composite; 5) Rupture of composite material; 6) Steel yielding. In the novel wrapped composite joints, thickness of the adhesive layer is negligible such that failure relative to it will not be taken into consideration. Therefore, the possible failure modes in this kind of joints are: 1) Rupture of composite material; 2) Delamination of composite; 3) Debonding at the bonded interface; 4) Yielding of steel tubes.

In the past few years, there have been many experimental studies devoted to characterize bonding behavior of composite-to-steel bonded joints with utilization of carbon fibre composites [18–31]. However, a huge knowledge gap exists concerning experimental characterization of static behavior of wrapped composite joints with utilization of glass fibre composites and introduction of extremely thin bond line.

This paper, following the previous research studies in TU Delft [14–16], focuses on 1) quantifing stiffness, elastic limit and ultimate load of wrapped composite joints vs welded counterparts under various load conditions; 2) Identifying governing failure modes and load transfer mechanism of wrapped composite jonts; 3) Understanding differences in failure modes at two different scales to predict upscaling capacity of wrapped composite joints. X-Joint geometry in two scales, diameter of brace/chord members Ø60 mm/108 mm and Ø219 mm/324 mm; two different angles between the brace and chord member: 45° and 90°; are tested with 3 monotonic load cases applied as tension, compression and in-plane-bending until failure. Deformation of the joint during loading is captured by observing surface strain measurements made by 3D digital image correlation (DIC) technique.

2. Ultimate load joint experiments

In offshore jacket structures, K-joint geometry is representative for connection between the chord and brace members. Due to difference in diameter of the chord and the brace, existence of gap and load transfer under an angle, this joint geometry is prone to tensile fatigue failure. Considering loading protocol limitations and efficiency of experiments in the laboratory, 2Y 45° joints and 2 T joints are finally used in tensile and in-plane bending experiments, respectively. 2Y 45° joint geometry with diameter ratio $d_1/d_0 = 60$ mm/108 mm = 0.56 resembles typical K-joints in terms of stress concentrations. In comparison, 2 T joints can be regarded equivalently as two identical T joints, and their geometry is helpful to set up in-plane bending experiments. For simplification of representation of experimental results, 2Y 45° joints and 2 T joints are called 45° X joints and 90° X joints, respectively, afterwards in this paper. Small-scale joint geometry is determined by downscaling the actual size joint geometry to 1/12 due to limitations of laboratory machines in terms of loading capacity and clamping devices. At small scale, 45° and 90° X joints connected by composite wrap and welding are compared in tensile and in-plane bending experiments, respectively, for stiffness, elastic limit and ultimate load comparisons. Wrapped composite X joints 45° at the small scale are also loaded in compression to investigate differences in tension vs compression in terms of joint resistance and governing failure mechanism. In order to investigate upscaling capacity, 45° wrapped composite X joint is upscaled by approximately four times of the brace diameter to medium scale in tensile experiments, reaching almost 1/3 of the actual scale as the first upscaling step for the novel wrapped composite joints.

2.1. Test series

Based on the above-mentioned motivation of the experimental campaign, 6 series of wrapped composite or welded X joint specimens are designed in the static experiments, as summarized in Table 1. Joints

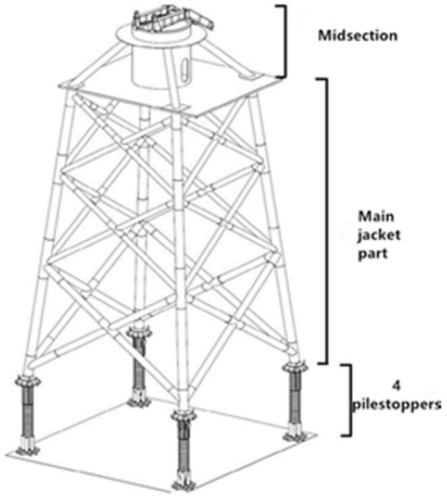

a) Off-shore wind turbine jacket supporting structures

b) Support structures of hydraulic barriers

c) Truss steel bridges

Fig. 1. Engineering application of CHS.

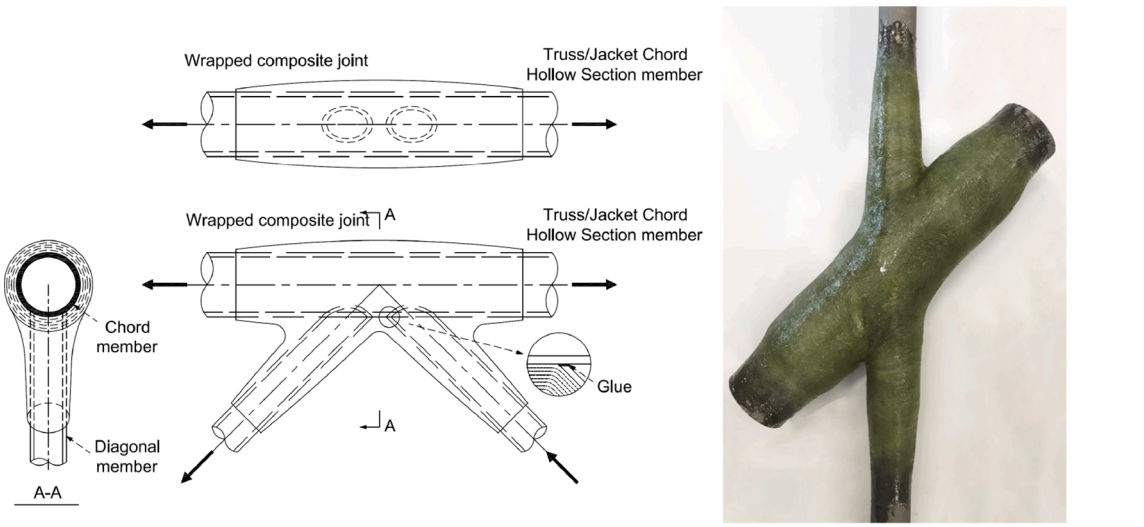

a) General configuration – example K-joint geometry b) 45° small-scale X joint specimen with Ø 60.3mm braces

Fig. 2. Wrapped composite joints.

Table 1
Test series and specimen naming.

Series number	Test series and specimen naming	Scale	Load condition	Connection type	Geometry in Figure number
1	cX45-Ss-T_S1/2/3/4/5	Small-scale	Tensile on braces	Composite	3(a)
2	wX45-Ss-T_S1/2	Small-scale	Tensile on braces	Welded	3(b)
3	cX45-Ss-C_S1/2/3	Small-scale	Compressive on braces	Composite	3(a)
4	cX90-Ss-B_S1/2	Small-scale	Bending on braces	Composite	3(c)
5	wX90-Ss-B_S1/2	Small-scale	Bending on braces	Welded	3(d)
6	cX45-Ms-T_S1/2/3	Medium-scale	Tensile on braces	Composite	4

with two different angles between braces and the chord member: 45° and 90°; in 2 geometric scales: small-scale and medium-scale are tested with 3 load cases applied as tension, compression and in-plane bending. Following naming convention is used for series given in Table 1, presented in Figs. 3 and 4 and used afterwards in analysis of the results: cX45/90 – wrapped composite joint, X geometry at 45°/90° angle; wX45/90 – welded joint, X geometry at 45°/90° angle; Ss, Ms – small-scale and medium-scale, respectively; T, C or B – tension, compression or in-plane bending loading on braces, respectively; S1/2/3/etc. - nominally identical specimens, number 1, 2, 3, etc.

Geometry with dimensions of CHS joints in Table 1 are shown in Figs. 3 and 4. 45°/90° X joints in small-scale are composed of two CHS 60.3/4 brace members and one CHS 108/5 chord member. 45° X joint in medium-scale consists of two CHS 219/6 brace members and one CHS 324/10 chord member. The dimensions of the medium-scale specimens are 30% of the real-scale in off-shore jacket supporting structures for wind turbines, where the brace and chord members are typically within 600 ~ 1200 mm range in diameter. X joints in small-scale are connected by either traditional welding technique or by wrapped composite joining (bonding through the composite wrap – i.e. no welding). Chord and brace members in X joints of medium-scale are only connected by wrapped composite joining.

Each series of wrapped composite joints loaded in tension and compression (series 1, 3 and 6) is accomplished with at least 3 nominally identical specimens to characterize scattering of static behavior of this new joining technology. Counterpart welded joints loaded in tension (series 2) are tested with at least 2 nominally identical specimens per series for the comparison reasons. Bending experiment (series 4 and 5) is

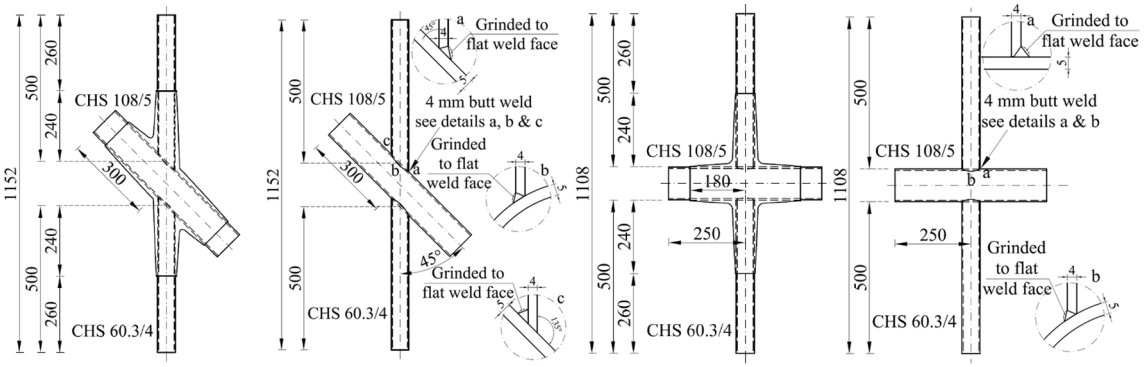

(a) cX45-Ss-T/C (series 1 and 3) (b) wX45-Ss-T (series 2) (c) cX90-Ss-B (series 4) (d) wX90-Ss-B (series 5)

Fig. 3. Geometry of 45°/90° small-scale wrapped composite and welded X joint specimens for tensile/compressive/bending tests.

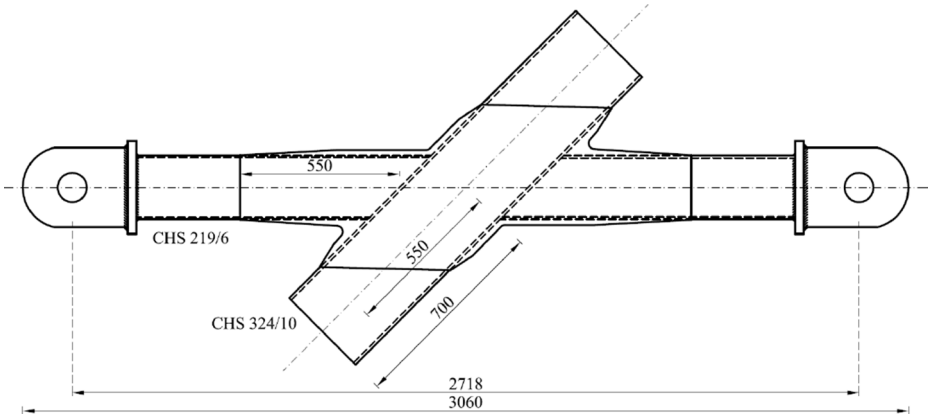

Fig. 4. Geometry of 45° medium-scale wrapped composite X joint specimens for tensile test (cX45-Ms-T; series 6).

accomplished with 2 specimens per series but 4 results are obtained from each series. That is because the clamped boundary conditions with 2 load point set-up allow almost independent test of bending on the left and the right brace members, which is explained in Section 2.3.3.

Three main objectives of the static experiments are defined:

a) to identify governing failure modes, load transfer mechanism, elastic limit and ultimate load of wrapped composite joints at various load conditions;
b) to compare tensile and bending static behavior of wrapped composite joints vs. welded counterparts;
c) to understand differences in failure modes at two different scales (small-scale and medium-scale) to predict upscaling capacity of the wrapped composite joints.

2.2. Material properties

The CHS profiles of all specimens are made of mild steel with grade S355. For welded X joints, the brace and chord members are connected by single-sided full penetration weld with 4-mm thickness followed by grinding weld toes to improve fatigue endurance, as shown in Fig. 3. For wrapped composite joints, CHS tubes are connected by E-Glass fibre mixed with vinyl ester based thermoset resin with volumetric fraction ranging 30–32% and wrapped (laminated) around steel hollow sections. It should be noted that the composite wrap is directly bonded on the steel tubes without application of intermediate adhesive layer so that the failure mode related to adhesive is eliminated. Steel tubes are grit blasted and chemically degreased as surface preparation prior to wrapping to ensure good bonding strength between the composite wrap and the steel tubes. The production process of wrapped composite joints is made in a controlled factory environment at room temperature and humidity conditions. The hand lamination (wrapping) procedure is fulfilled in a couple of stages with quality control to ensure good compaction and avoiding air gaps. The thickness of the composite wrap is maximum at the joint root with a value of 14 mm and 23 mm in small and medium-scale, respectively, and decreases to 0 mm at the end of the bonded connection, see Figs. 3 and 4. No post-curing is applied to the wrapped specimens. Mechanical properties of the composite wrap laminate are summarized in Table 2. They are quantified by standard tensile/compressive/in-plane shear coupon tests in room conditions in terms of temperature and humidity, and the geometry of the coupon is determined based on ISO standards [32–34] for quasi-isotropic composite laminates.

Table 2
Mechanical properties of the composite wrap laminate.

Mechanical properties	Average value (and CoV [%])
In-plane compressive strength in x/y direction – $f_{x,c} = f_{y,c}$	200 MPa (3.79)
In-plane compressive modulus in x/y direction – $E_{x,c} = E_{y,c}$	12077 MPa (4.50)
In-plane tensile strength in x/y direction – $f_{x,t} = f_{y,t}$	216 MPa (5.78)
In-plane tensile modulus in x/y direction – $E_{x,t} = E_{y,t}$	11798 MPa (6.37)
In-plane major Poisson's ratio – ν_{xy}	0.15 (6.50)
In-plane shear strength – $f_{xy,v}$	72.2 MPa (2.59)
In-plane shear modulus – G_{xy}	3120 MPa (6.81)

2.3. Experimental set-up

2.3.1. Small-scale 45° X joints under tensile and compressive load

The tensile and compressive experiments of 45° X joints in small-scale are conducted in the Universal Testing Machine (UTM) with 800 kN loading capacity equipped with hydraulic clamping heads in Stevin lab 2 of TU Delft, as shown in Fig. 5. The axial load on braces is applied through gripping the ends by pairs of preloaded steel clamps with pins inside, as shown in Fig. 5d), in order to obtain uniform stress distribution in cross section at load introduction. Load is applied by displacement control with rate of 1 mm/min to provide quasi-static loading condition.

2.3.2. Medium-scale 45° X joints under tensile load

The tensile test of 45° X joints in medium-scale is conducted in the 6-meter-high loading frame with 2.5 MN loading capacity, as shown in Fig. 6a) and b). The specimen is pin connected to the loading frame through the ear plates with Ø100 mm cylindrical hole, which are welded through end plates to the braces. Load is applied by controlling the hydraulic jack moving upward, with the displacement control with rate of 1 mm/min to obtain quasi-static loading condition.

2.3.3. Small-scale 90° X joints under bending load

The in-plane bending load is applied to 90° small-scale X joint specimens through lateral load on braces. Two synchronized hydraulic jacks with load capacity of 100 kN are eccentrically connected to brace ends at 450 mm away from the chord center, each. The lateral load on the brace is applied through set of preloaded wooden clamps to prevent local buckling of the cross section at the load introduction, see Fig. 6c) and d). The chord member in the middle is fixed to the frame by applying preload at the top and bottom cross section. Such clamped boundary conditions with 2 load point set-up allows independent test of bending on the left and the right brace members. Load is applied simultaneously with displacement control of 1 mm/min. Once one of the connections of the left or the right brace member fails due to the excessive bending, the load is continued on the opposite side. Therefore, from one specimen two bending test results are obtained.

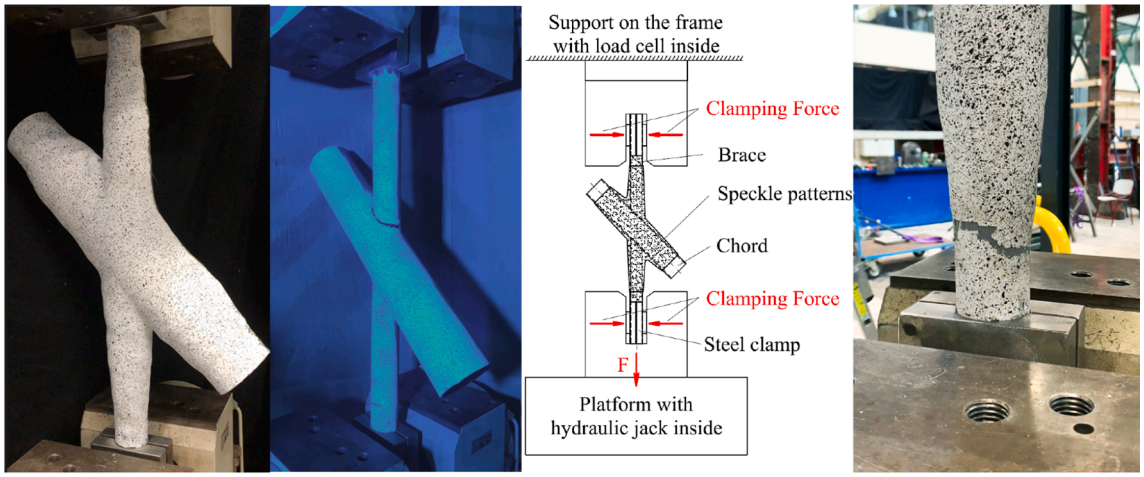

a) Wrapped composite joint b) Welded joint c) Small-scale tension set-up (d) Load application at brace end

Fig. 5. Test set-up of small-scale 45° X joints under tensile/compressive axial load.

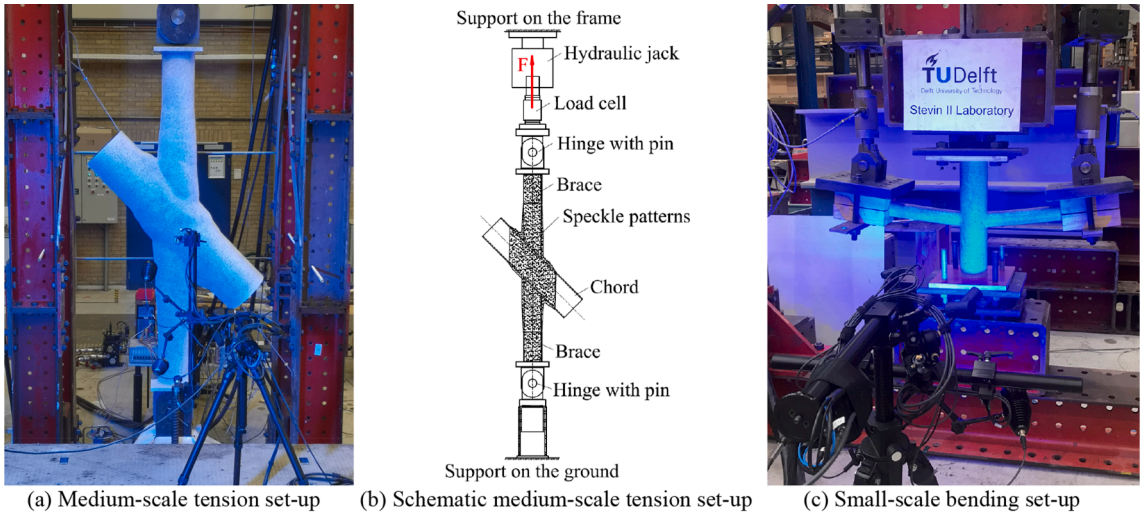

(a) Medium-scale tension set-up (b) Schematic medium-scale tension set-up (c) Small-scale bending set-up

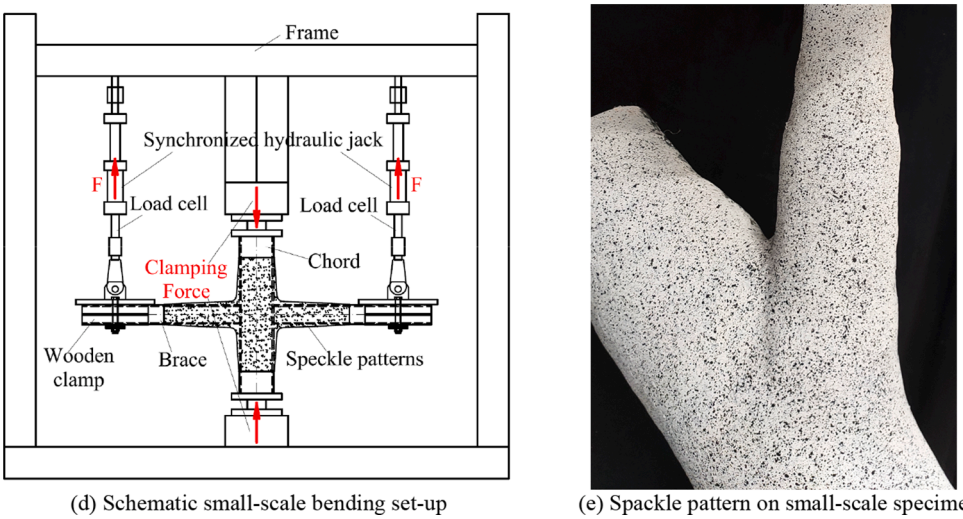

(d) Schematic small-scale bending set-up (e) Spackle pattern on small-scale specimens

Fig. 6. The 3D DIC system with live measurement of displacements and strains on the surface of specimen at two scales.

2.4. Measurement set-up

A 3-dimensional (3D) Digital Image Correlation (DIC) system is utilized to measure global displacement and surface strain of the specimens, as shown in Fig. 6. GOM Aramis adjustable base 12MPx system is used which includes two cameras with 12-megapixel resolution,

controller and graphical analysis software to acquire and process test data. It enables recording of strain distribution and crack initiation/propagation on the specimen surface during the experiments, and processing of measurement data with high accuracy and pertinence after the experiments.

Two measuring volumes are used corresponding to wrapped composite joints in two geometric scales. The 1900 × 1400 × 1400 mm^3 measuring volume is utilized in the medium-scale test, while the 750 × 610 × 610 mm^3 measuring volume is used in the small-scale tension, compression and bending tests. Speckle patterns are applied on the specimens' surface by spray method with grain size of approximately 2 and 4 mm in small-scale and medium-scale experiments, respectively. Polarized blue light is used to limit influence of variation of ambient light on measurement accuracy.

3. Failure modes of wrapped composite joints

Based on the results of preliminary tensile static tests [14–16] and the results shown in this paper afterwards, the load transfer mechanism and potential failure scenarios of wrapped composites joints are identified and schematically shown in Fig. 7. The main load transferring components of the wrapped composite joint are:

- Primary bonded interface – which connects the brace members to the composite wrap. The joint load (tension, compression, bending) from the steel brace member is transferred to the composite wrap mainly through mode II (shear) interface behaviour.
- Composite wrap – which transfers the joint load from the brace members to other brace members and to the chord. The load transfer is through complex multi-axial stress state at the *meso*-scale, scale of the curved laminate.
- Secondary bonded interface – which connects the composite wrap to the chord member. The load transfer is through mixed-mode interface behaviour, i.e. combination of Mode I (peel) and Mode II/III (shear).

The failure modes of the wrapped composite joint can be divided into four main groups for any general load direction:

1) Failure of the primary bonded interface by partial of full debonding. Mode II interface failure is dominant, partially reduced by mode-mixity with Mode I interface stresses at the root due to local bending of the composite wrap. The crack initializes at the root of the connection (coincidence of the brace and chord) due to stress concentrations. Thickness profile of the composite wrap is tapered towards the wrap end to reduce the stress concentrations.
2) Failure of the composite wrap by fracture involving micro-scale failure modes of the fibres and resin. The failure criterion of composite material was adopted to be 1.2% from looking at the surface strain in DIC results. Given the quasi-isotropic behaviour and relatively large thickness (up to 23 mm) of composite wrap laminate used in the joints, the local failure modes of the composite wrap can be characterized as: a) in-plane tensile / compressive / shear failure of the laminate and b) out-of-plane shear and tensile failure of the laminate due to delamination.
3) Failure of the secondary bonded interface by debonding of the composite wrap from the steel chord member. The mode-mixity of Mode I and Mode II/III failure behaviour at the interface connecting the composite wrap to the chord member will depend on ratio of diameter of the chord and the brace. With smaller brace-to-chord diameter, the peel stresses (Mode I) can turn dominant for example in case of tensile joint load on the brace as the composite wrap is pulled away from the chord.
4) Failure of steel brace member by yielding or local buckling next to, or inside the composite wrap. Yielding of the steel inside the composite wrap can promote debonding on the primary bonded interface. Yielding of the steel outside, close to the end of composite wrap can initiate debonding crack from the end of the primary bonded interface.

The interaction of failure modes of separate components can lead in general to two scenarios:

Loss of structural integrity (failure): due to full debonding on primary bonded interface and/or failure of the composite wrap in a complete circumference around any brace member. The transfer of the joint loads between the brace members and between the chord and the brace members is no longer possible.

Secant stiffness degradation: Partial debonding on the secondary bonded interface will not lead to loss of structural integrity of the joint but will result in loss of joint secant stiffness. It will be shown in the results of small-scale and medium-scale experiments that debonding on the secondary bonded interface is only partial. Even in a very unlikely event of failure of the entire bonded interface on the chord there would not be loss of structural integrity of the joint. The transfer of the joint load components between the brace members and partially to the chord would still be possible through the composite wrap. Also, partial debonding on primary bonded interface leads to reduction of secant stiffness of the joint but not to the loss of the structural integrity.

4. Results and discussion

General overview of all test results is given in Table 3. The indicated failure modes and scenarios of failure and stiffness degradation are presented through the experiment results for various load cases and scales. Identification of failure modes is facilitated by analysis of surface strains obtained by 3D DIC measurements in combination with general load displacement curves.

4.1. Small-scale 45° X joints under tensile load

Fig. 8 shows the load–displacement curves of 5 wrapped composite joint specimens vs 2 welded counterparts in small-scale loaded in

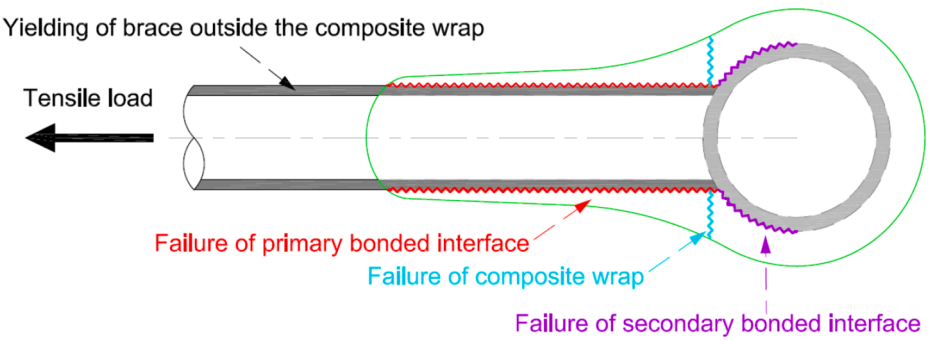

Fig. 7. Load transfer mechanism of a wrapped composite joint loaded in tension.

Table 3
Test results.

Specimen	Initial stiffness [kN/mm]	Elastic load limit [kN]	Ultimate load [kN]	Final failure mode
cX45-Ss-T_S1	159.0	183.9	339.5	Primary bonded interface with yielding of brace
cX45-Ss-T_S2	163.3	182.2	346.5	Primary bonded interface with yielding of brace
cX45-Ss-T_S3	160.3	180.5	347.4	Primary bonded interface with yielding of brace
cX45-Ss-T_S4	171.9	180.4	350.0	Primary bonded interface with yielding of brace
cX45-Ss-T_S5	170.3	184.9	344.9	Primary bonded interface with yielding of brace
Average (and COV [%])	164.9 (3.15)	182.4 (0.98)	345.7 (1.01)	
wX45-Ss-T_S1	125.6	156.7	334.1	Punching shear failure of the chord next to welds
wX45-Ss-T_S2	129.0	153.3	341.9	Punching shear failure of the chord next to welds
Average (and COV [%])	127.3 (1.37)	155.0 (1.09)	338.0 (1.16)	
cX45-Ss-C_S1	177.4	215.2	361.2	Local buckling of brace
cX45-Ss-C_S2	177.8	221.3	358.2	Primary bonded interface with yielding of brace
cX45-Ss-C_S3	166.0	223.5	361.7	Local buckling of brace
Average (and COV [%])	173.7 (3.14)	220.0 (1.60)	360.4 (0.42)	
cX45-Ms-T_S1	349.2	1193	1483	Primary bonded interface without yielding of steel
cX45-Ms-T_S2	345.2	1139	1353	Primary bonded interface without yielding of steel
cX45-Ms-T_S3	341.5	1053	1640	Primary bonded interface with yielding of steel
Average (and COV [%])	345.3 (0.92)	1128 (5.11)	1492 (7.88)	
cX90-Ss-B_S1_Left	4.01	10.81	36.59	Fracture of wrap root in the tensile zone
cX90-Ss-B_S1_Right	3.68	10.26	38.03	Fracture of wrap root in the tensile zone
cX90-Ss-B_S2_Left	3.63	10.04	33.66	Fracture of wrap root in the tensile zone
cX90-Ss-B_S2_Right	3.35	10.10	32.02	Fracture of wrap root in the tensile zone
Average (and COV [%])	3.67 (6.42)	10.30 (2.93)	35.07 (6.74)	
wX90-Ss-B_S1_Left	2.29	7.16	18.92	Brace failure next to welds in the tensile zone
wX90-Ss-B_S1_Right	2.41	7.18	18.47	Brace failure next to welds in the tensile zone
wX90-Ss-B_S2_Left	2.39	7.19	19.84	Brace failure next to welds in the tensile zone
wX90-Ss-B_S2_Right	2.31	7.11	19.61	Brace failure next to welds in the tensile zone
Average (and COV [%])	2.35 (2.22)	7.16 (0.43)	19.21 (2.84)	

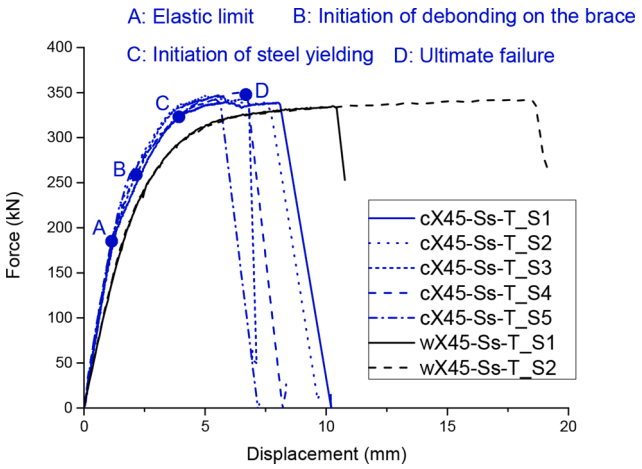

Fig. 8. Tensile behavior of 45° small-scale wrapped composite joint specimens vs welded counterparts.

tension. Wrapped composite joint specimens in this case show 30% larger initial stiffness, 18% larger elastic load limit and 3% larger ultimate load resistance than welded counterparts, with low scattering within 0%~5% range. Ultimate displacement at failure is lower compared to welded counterparts, however with less scattering. The elastic load limit of wrapped composite joints (180 kN) is 51% higher than the nominal resistance of the counterpart welded joints (119 kN) calculated according to EN 1993-1-8 [35]. Full debonding on the primary bonded interface and final pull-out of steel brace member from the composite wrap is predominant failure mode in wrapped composite joints, See Fig. 5d). Welded joints are characterized by punching shear failure of the chord next to welds initiating from the joint crown toe and developing into the joint crown heel, see Fig. 5b).

Fig. 9 gives the explanation of physical analogy that is used to determine the debonding crack length by using longitudinal surface strains obtained from DIC in experiments. In the perfectly bonded state, steel and composite in an arbitrary cross section are connected and carry the external force in a hybrid manner. The longitudinal strains along the steel brace and the composite wrap are of similar magnitude. Therefore, the distribution of surface strain along the path is relatively uniform with a steady increase towards the root due to local bending caused by transfer of load to the chord. In the partial debonded state, by contrast, an instantaneous jump of surface strain will appear on the surface of composite near the crack tip because there is only composite material part of the cross section carrying the external load at the debonded part of the primary bonded interface.

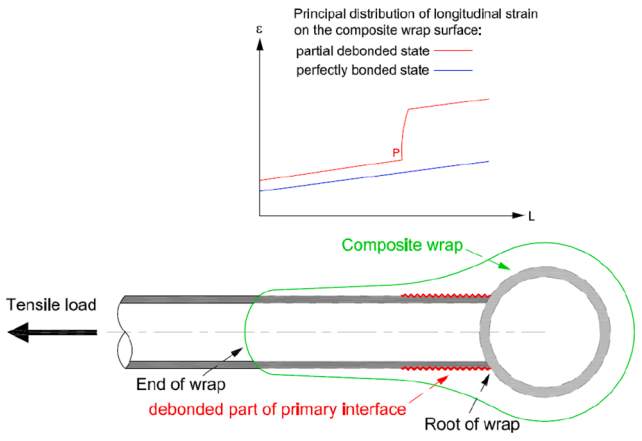

Fig. 9. The approach of using the distribution of longitudinal surface strains to determine debonding crack length on the brace.

Surface strains (principal strains) of a representative wrapped composite joint specimen (cX45-Ss-T_S4) are presented in Fig. 10 at critical load stages identified in load–displacement curve to explain the failure process. Wrapped composite joints behave elastic as shown in Fig. 10a) until 180 kN (point A) which corresponds to 52% of the ultimate tensile load of 350 kN on braces. The end of linear elastic behavior is attributed to initiation of debonding on the secondary bonded interface between the composite wrap and the chord member due to combination of concentrated peel and shear stress on the interface. This is indicated by localized increase of surface strains in Fig. 10b) in contrast to Fig. 10a) in the region of the composite wrap on the chord next to the brace. This process is gradual in contrast to behavior in tensile experiment at the larger (medium)-scale shown later, probably due to the relatively large ratio between the wrap thickness and the tube diameter in small-scale joints. Gradual increase of debonding on the secondary bonded interface is followed further by initiation of debonding on the primary bonded interface between the composite wrap and the brace members at 258 kN (point B), as shown in Fig. 10c). Debonding crack propagates steadily from the joint root. Additional debonding crack is initiated on the primary bonded interface from outside of the connection at the load stage of 321 kN (point C) when steel cross section at the end of the composite wrap contracts due to yielding (see Fig. 10d)). Once steel brace has yielded sufficiently, the load transfer on primary bonded interface is exhausted and fails completely when it is shortened to a critical bonding length at load level of 346 kN (point D), as shown in Fig. 10e).

A path is defined in the middle of the brace member, starting at the free end of the composite wrap and ending at the root connection to the chord, as indicated in Fig. 10. The longitudinal surface strains along the path obtained at characteristic loading stages are shown in Fig. 11. The aim is to identify indirectly the debonding crack length by observing local increase of surface strains at the crack front. Surface strains distribute uniformly, without steep increase along the path, in the linear elastic stage, load level of 170 kN before point A indicated in Fig. 8. Slight increase of strain near the joint root at the early stage of inelastic behavior (225 kN) is the consequence of debonding on the secondary bonded interface because it is connected to the primary boned interface at the root of the joint. Significant steep increase of surface strain from 0.3% to 0.6% indicates that debonding is initiated on the primary bonded interface with 20 mm debonding length at load level 258 kN (point B) which is a later stage of inelastic behavior. Debonding length at the root steadily increases to 62 mm at the load level 321 kN

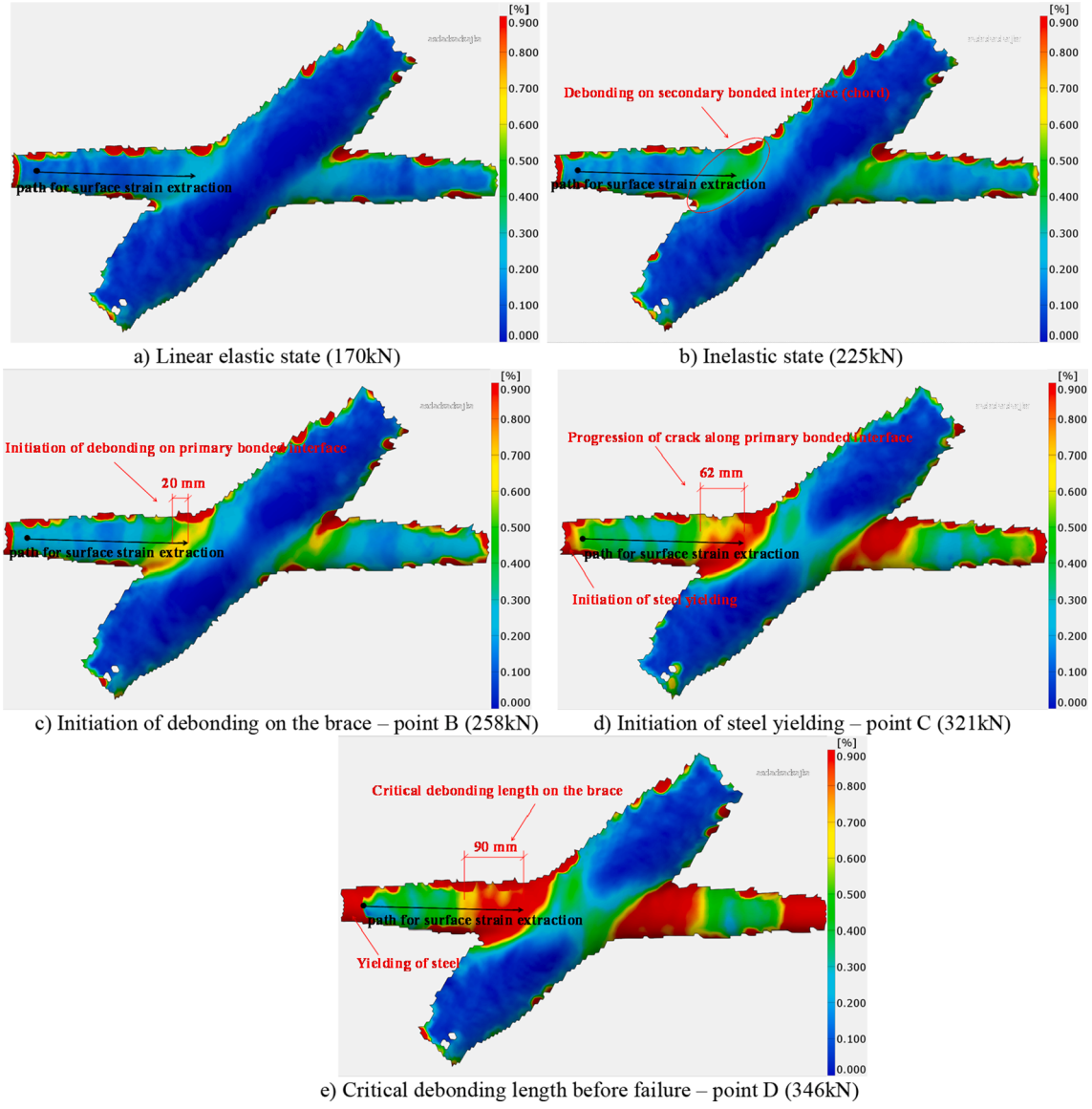

Fig. 10. Surface strains of cX45-Ss-T_S4 at critical loading stages indicating failure process.

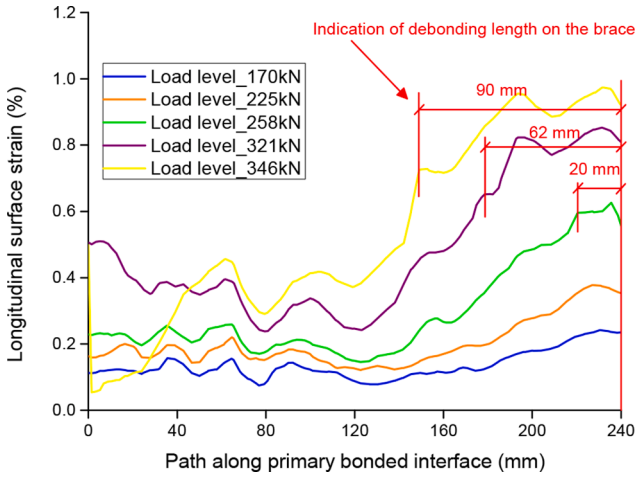

Fig. 11. Longitudinal surface strains along primary bonded interface at characteristic loading stages.

corresponding to initiation of yielding of steel – point C in Fig. 8. In summary, the gradual loss of secant stiffness during the inelastic stage, between points A and C, is attributed to initiation and growth of the debonding on the secondary bonded interface on the chord and the primary bonded interface on the brace up to 62 mm (26% of full bonding length). The critical length of the debonding crack on the brace of 90 mm (38% of full bonding length) is recorded just before ultimate failure (see Fig. 11) when it coalesces with the crack initiated at the end of the composite wrap due to excessive yielding of steel.

4.2. Small-scale 45° X joints under compressive load

Fig. 12 compares load–displacement curves of wrapped composite joint specimens loaded in compression vs tension (shown in previous section). Wrapped composite joint specimens loaded in compression show 5% larger initial stiffness, 21% larger elastic load limit and 4% larger ultimate load than in tension. The elastic load limit of wrapped composite joints in compression (215 kN) is 81% higher than the nominal resistance of the counterpart welded joints (119 kN) calculated according to EN 1993-1-8 [35]. In the compressive test, all three specimens have the same ultimate load level, and their bonding resistance is all higher than the yielding resistance of the brace cross section confirmed by DIC data. In two out of three specimens (cX45-Ss-C_S1 and C_S3), the bonding resistance is slightly higher, leading to full plastic buckling of the brace cross section outside the wrapped region (see Fig. 15). By contrast, in specimen cX45-Ss-C_S2, the bonding resistance is a bit lower, allowing the compressive yield strains at the end of the composite wrap to progress inside the composite wrap. Progression of yield strains inside the composite wrap initiates coalescence of the debonding crack from the wrap end and the wrap root, leading to full debonding as in the case of the tensile experiment. Some specimens show slight drops of load in load–displacement curves, which is attributed to the interaction between debonding on the secondary bonded interface and ovalization of the chord due to contact force from the brace.

Surface strains (principal strains) of a representative wrapped composite joint specimen (cX45-Ss-C_S1) are presented in Fig. 13 at critical load stages identified in load–displacement curves to explain the failure process. The colors in compression DIC images (Fig. 13) corresponds to the same absolute values of strain as in tension DIC images in Fig. 10. Additional load transferring mechanism exists in the joints loaded in compression through the direct contact between the brace and the chord member at the root of the joint. This is identified as main reason for higher limit of elastic behavior at 215 kN (point A in load–displacement curve) compared to joints loaded in tension. The debonding on the secondary bonded interface leads to gradual decrease of secant stiffness from point A to C in the load–displacement curve. Debonding on primary bonded interface, see Fig. 13c), is also initiated at slightly higher load level (295 kN, point B) compared to tensile experiment which is again consequence of partial load transfer through the direct contact inside the joint. Progression of debonding on the primary bonded interface (brace) until point C (323 kN, Fig. 13d)) when steel starts to yield is also less compared to tensile experiment. The ultimate load is reached at 359 kN (point D) when local buckling of steel outside of the composite wrap is initiated and leads to reduction of load (point E, Fig. 13e)).

The distribution of longitudinal surface strains in Fig. 14 clearly

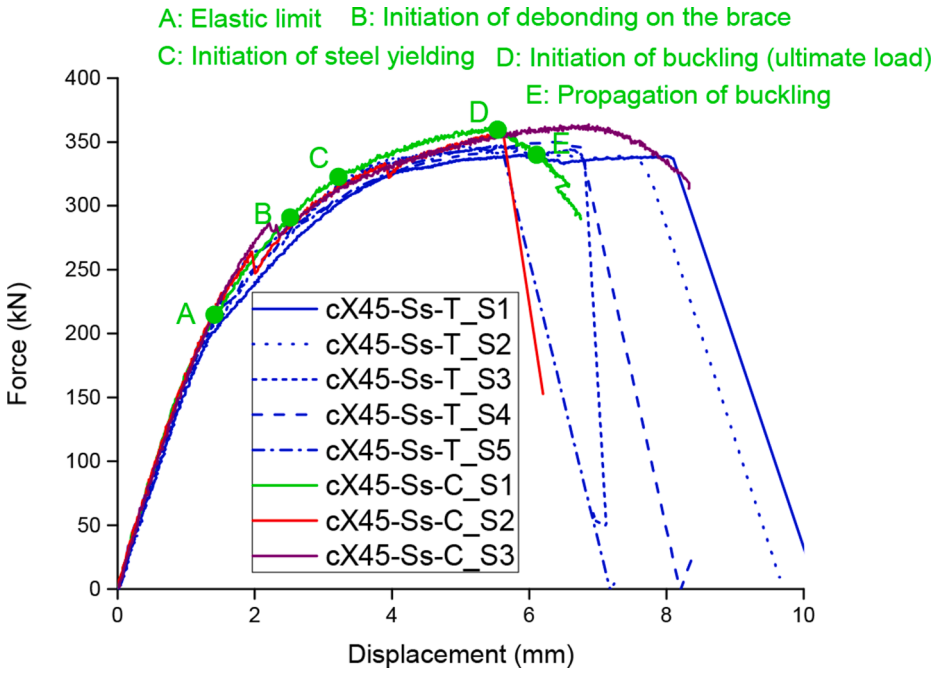

Fig. 12. Compressive vs tensile behaviour of 45° small-scale wrapped composite joint specimens.

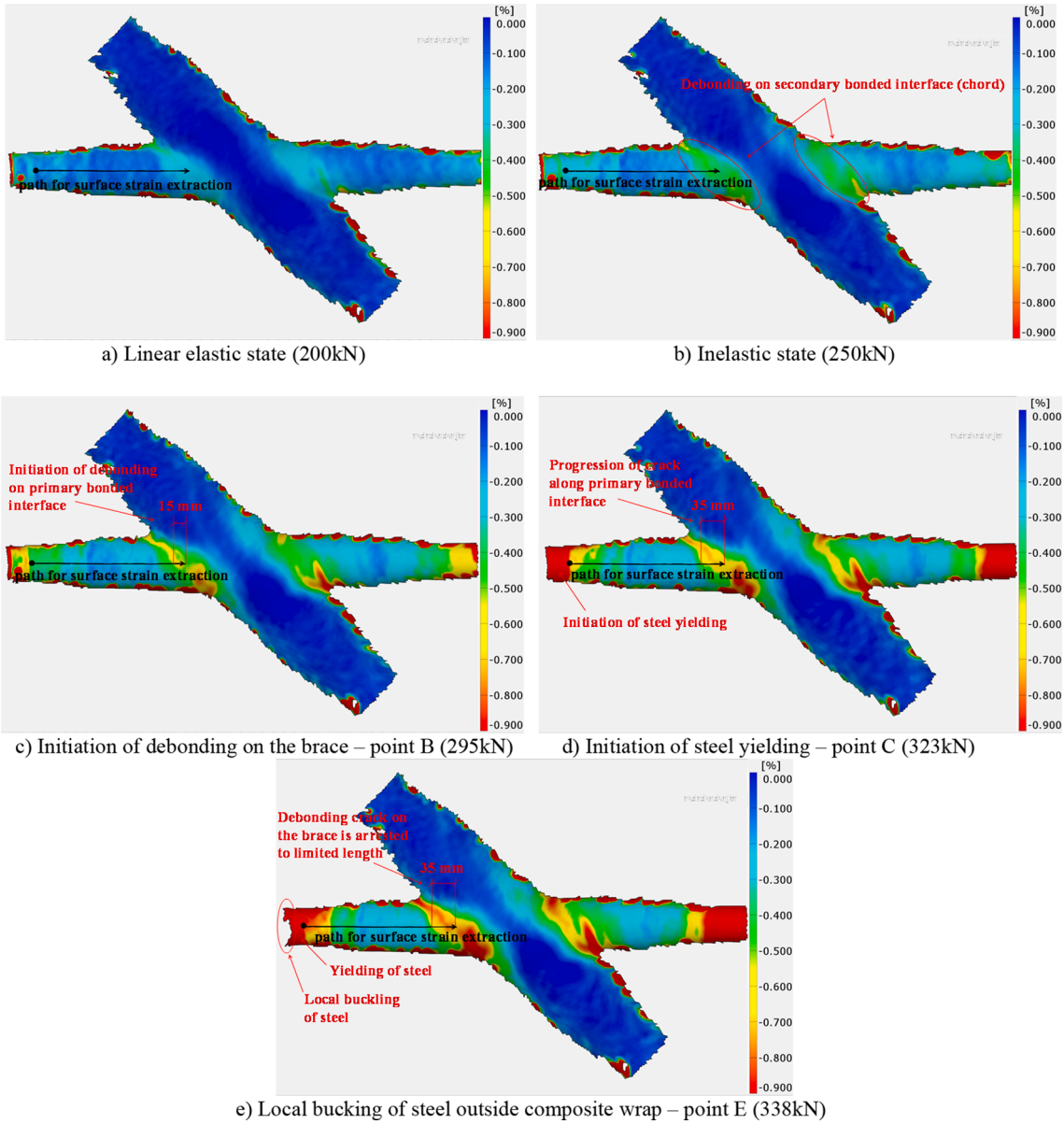

Fig. 13. Surface strains of cX45-Ss-C_S1 at critical loading stages indicating failure process.

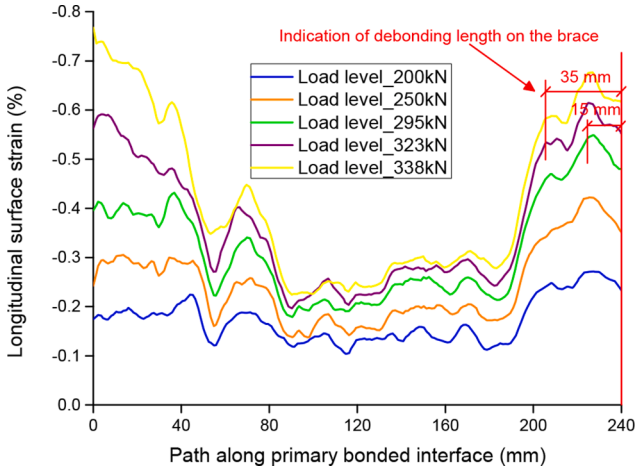

Fig. 14. Longitudinal surface strains along primary bonded interface at characteristic loading stages.

indicates that in contrast to tensile experiment, the debonding crack in the root at the primary bonded interface is arrested to limited length of 35 mm. The compressive strains at the end of the composite wrap linearly increase as a consequence of local buckling of brace CHS. The steel cross section is expanding in this case which prevents formation of peel stresses at end of the composite wrap.

4.3. *Medium-scale 45° X joints under tensile load*

Wrapped composite joint specimens in medium-scale show linear elastic behaviour in axial tension up to a minimum of 1053 kN, see point A in load–displacement curve of specimen cX45-Ms-T_S3 in Fig. 16. This elastic load limit of wrapped composite joint is 82% higher than the nominal resistance of the counterpart welded joints (577 kN) calculated according to EN 1993-1-8 [35]. Full debonding on the primary bonded interface and final pull-out of steel brace member from the composite wrap is predominant failure mode, accompanied by delamination at the root of wrap and at the end of wrap on brace, as shown in Fig. 17. Full debonding happens before yielding of the steel brace outside the composite wrap in two out of three specimens (cX45-Ms-T_S1 and S2) while

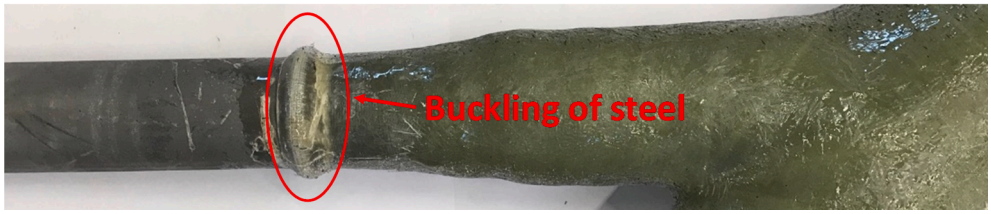

Fig. 15. Buckling of brace outside the composite wrap in compression test.

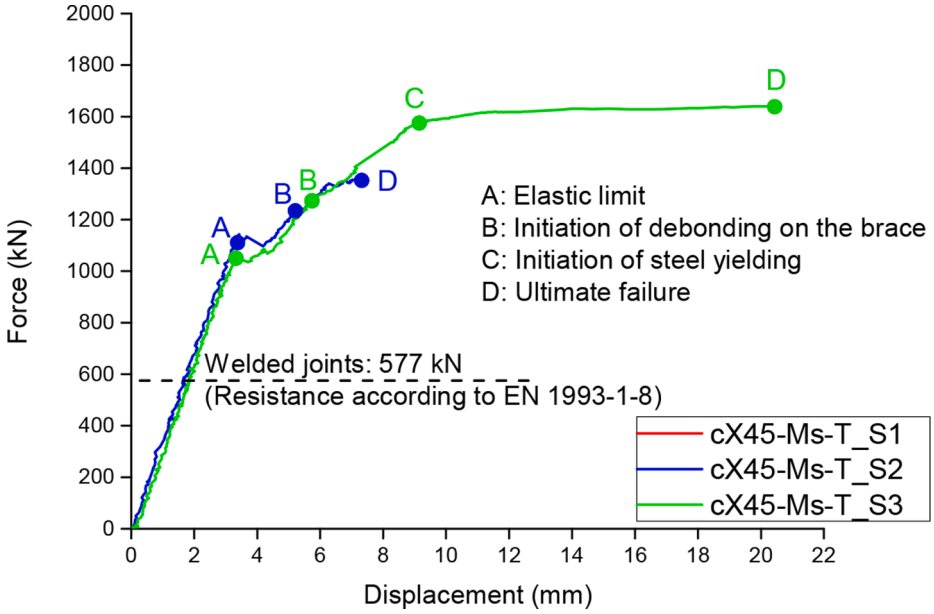

Fig. 16. Tensile behavior of 45° medium-scale wrapped composite joint specimens.

the ultimate load exceeds the yield resistance of steel brace CHS in specimen cX45-Ms-T_S3. The possible reason is better bonding quality in the last specimen.

Development of surface strains (principal strains) of 2 specimens, cX45-Ms-T_S2 and cX45-Ms-T_S3, are shown in Figs. 18 and 19, respectively. Critical load stages are identified in load–displacement curves to explain the two different failure process related to final debonding before or after yielding of steel brace. Comparison between Fig. 18a) and b) and between Fig. 19a) and b) indicates that initiation of non-linear behavior is caused by debonding on secondary bonded interface at 1139 and 1053 kN (64% of the ultimate load of cX45-Ms-T_S3) as shown in point A, respectively. This process is characterized by sudden debonding on relatively large area of the chord and drop of stiffness within 1050 ~ 1200 kN load range in contrast to tensile experiments at the small-scale shown in Fig. 9b) where the stiffness degradation is gradual. The difference in chord debonding behavior between the two scales is probably due to smaller ratio between the composite wrap thickness and the tube diameter in medium-scale compared to small-scale joints. Debonding on secondary bonded interface is followed by initiation of debonding on primary bonded interface at 1224 kN and 1248 kN (point B), as shown in Fig. 18c) and Fig. 19c), respectively. As for the specimen with lower bonding quality (cX45-Ms-T_S2), the debonding length on the primary bonded interface increases significantly to the critical value (240 mm) leading to final failure at 1346 kN (point D) before yielding of brace CHS, as shown in Fig. 18d). By contrast, Fig. 19d) indicates that the same debonding length is reached on the primary bonded interface at higher load level (1570 kN, point C) when brace starts to yield in the specimen with better bonding quality (cX45-Ms-T_S3). It is followed by final failure with longer critical debonding length (295 mm) reached at 1640 kN (point D) as shown in Fig. 19e).

Fig. 20 illustrates longitudinal surface strains of cX45-Ms-T_S3 along the path obtained at critical load stages in Fig. 19 to indirectly identify the debonding length on the primary bonded interface. Similar to small-scale test, strain is relatively uniform in the elastic and inelastic stage of medium-scale test. Debonding is initiated with 55 mm debonding length where strain increases considerably to 0.4% at 1248 kN (point B). Debonding length increases to 240 mm (44%) when yielding of steel is initiated at 1570 kN (point C) and subsequently reaches 295 mm (54%) just before final failure at 1640 kN (point D).

4.4. *Small-scale 90° X joints under in-plane bending load*

Fig. 21 shows the load–displacement curves of 2 wrapped composite joint specimens vs. 2 welded counterparts (4 results each) in small-scale subjected to in-plane bending load. Wrapped composite joint specimens in this case show 56% larger initial stiffness, 44% larger elastic load limit and 83% larger ultimate load than welded counterparts. The elastic load limit of wrapped composite joints (10 kN) is 6% higher than the nominal load resistance of the counterpart welded joints (9.47 kN), corresponding to the bending moment in the root of the brace calculated according to Wardenier [1]. Fracture of the composite wrap in the complete circumference around the brace member is predominant failure mode, see Fig. 22a). Meanwhile, partial debonding on primary bonded interface in the tensile zone and on the joint side and delamination in the compressive zone is observed, as shown in Fig. 23. Fig. 22b) indicates that welded specimens are characterized by bending fracture of the brace member next to the welds in the tensile zone, not the failure of the joints. This is confirmed by the fact that the ultimate bending resistance (7.49 kN.m) of the CHS cross section calculated

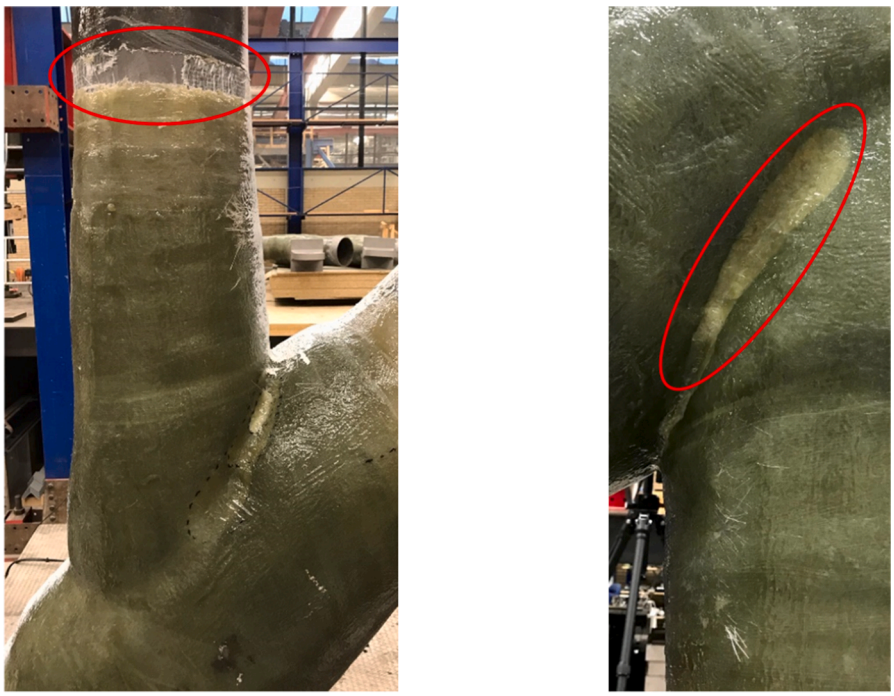

a) full debonding at the primary bonded interface and delamination at the end of wrap on brace

b) delamination at the root of composite wrap

Fig. 17. Failure patterns on 45° medium-scale wrapped composite joint specimens loaded in tension.

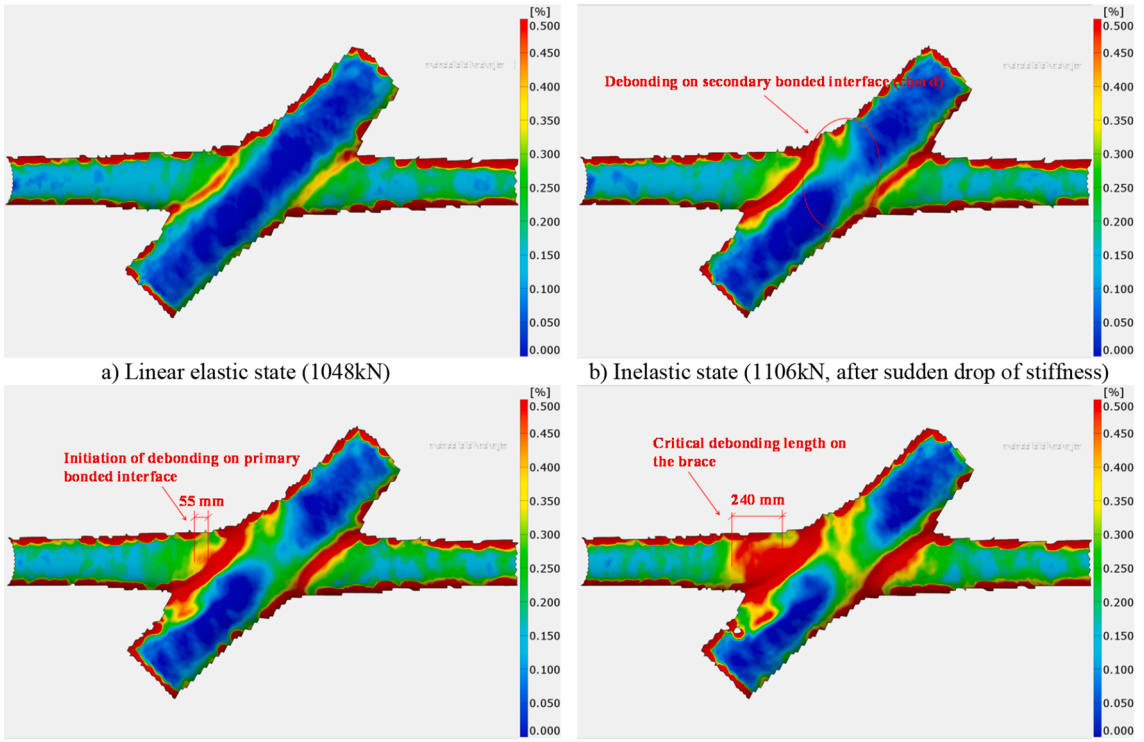

a) Linear elastic state (1048kN)

b) Inelastic state (1106kN, after sudden drop of stiffness)

c) Initiation of debonding on the brace – point B (1224kN)

d) Critical debonding length before failure – point D (1346kN)

Fig. 18. Surface strains of cX45-Ms-T_S2 at critical loading stages indicating failure process.

concerning the ultimate strength of steel (590 MPa [14]) corresponds to the bending moment in the joint root by applying the ultimate load (19 kN).

Surface strains (Principal strains) of a representative wrapped composite joint specimen (cX90-Ss-B_S2) are presented in Fig. 24 from DIC results at critical load stages identified in load–displacement curve to explain the failure process. Comparison between Fig. 24a) and b) indicates that initiation of inelastic behaviour of the joint is due to

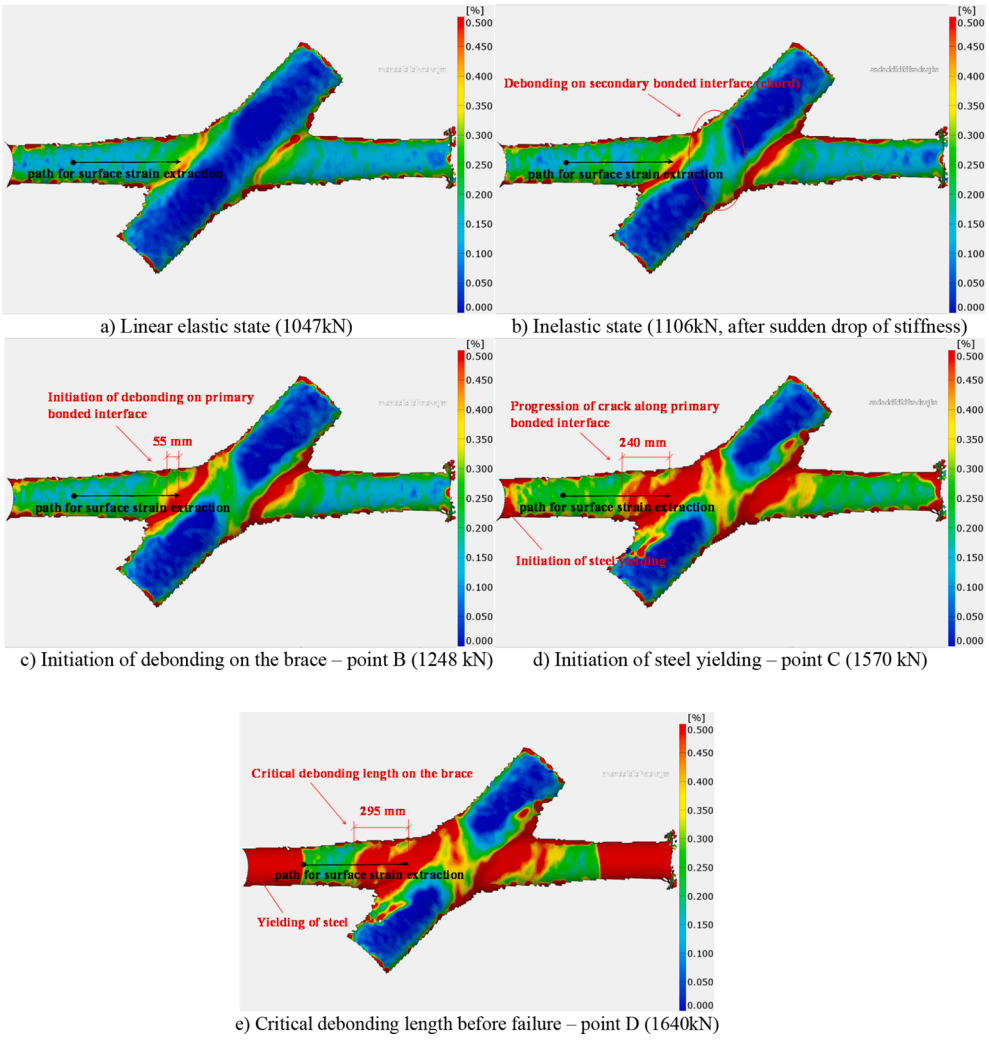

a) Linear elastic state (1047kN)
b) Inelastic state (1106kN, after sudden drop of stiffness)
c) Initiation of debonding on the brace – point B (1248 kN)
d) Initiation of steel yielding – point C (1570 kN)
e) Critical debonding length before failure – point D (1640kN)

Fig. 19. Surface strains of cX45-Ms-T_S3 at critical loading stages indicating failure process.

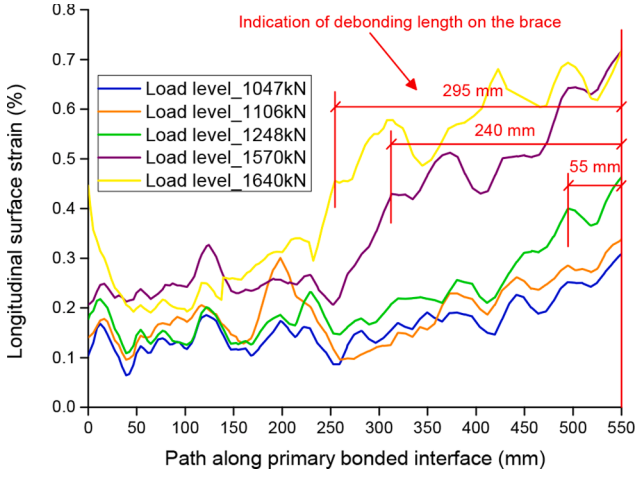

Fig. 20. Longitudinal surface strains along primary bonded interface of cX45-Ms-T_S3 at characteristic loading stages.

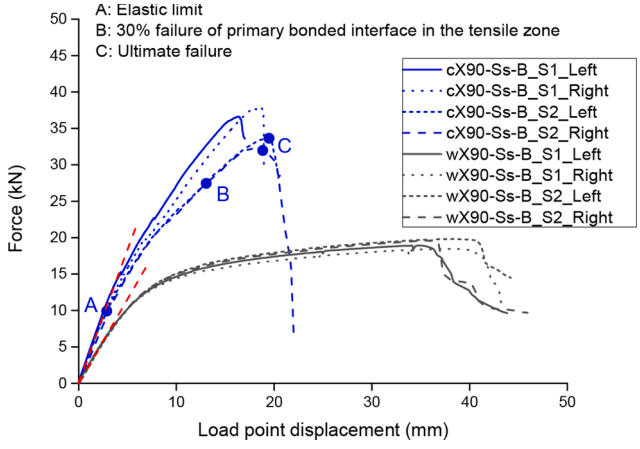

Fig. 21. Bending behavior of 90° small-scale wrapped composite joint specimens vs welded counterparts.

debonding on the secondary bonded interface (chord) in the tensile zone, when transverse bending load reaches 30% of the ultimate load (10 kN, point A). Subsequently, debonding on the primary bonded interface in the tensile zone and on the joint side will be initiated and propagate gradually to 80 mm (30% of the bonding length) at load level 27 kN (point B), as shown in Fig. 24c). Nevertheless, debonding on the brace will not further develop because fracture of the composite wrap happens in the circumference around the wrap root in the tensile zone and results in final failure at 33 kN (point C).

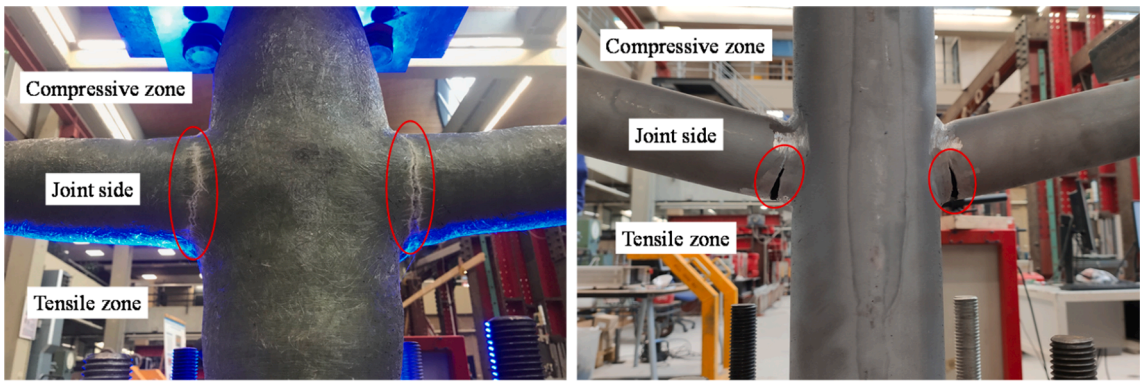

a) Wrapped composite joint b) Welded joint

Fig. 22. Failure pattern on 90° small-scale wrapped composite joint specimens vs welded counterparts.

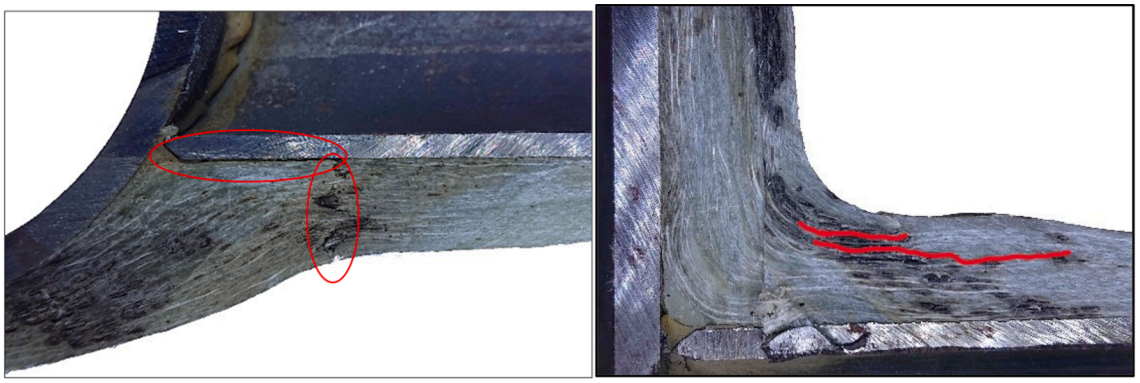

a) debonding on primary bonded interface and fracture of the composite wrap on the joint side b) delamination of composite wrap in the compression zone

Fig. 23. Cut-through 90° small-scale wrapped composite joint specimens loaded in bending.

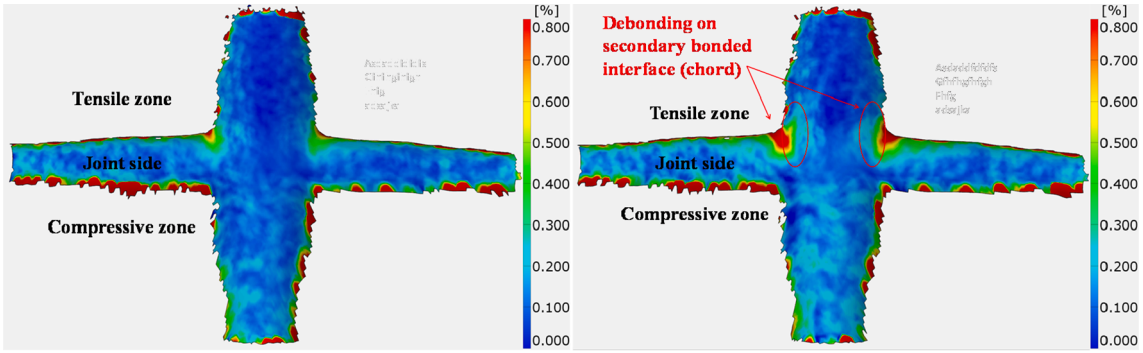

a) Linear elastic state (8kN) b) Inelastic state (14kN)

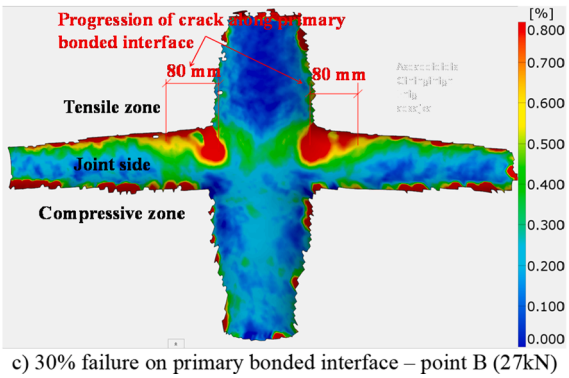

c) 30% failure on primary bonded interface – point B (27kN)

Fig. 24. Surface strains of cX90-Ss-B_S2 at critical loading stages indicating failure process.

5. Conclusions

Six series of ultimate load experiments were conducted to characterize failure process and failure modes of wrapped composite joints connecting steel CHS brace members to chord members solely through bonding as alternative to welded CHS joints. X joint geometry was chosen as stringent for the joint performance due to known large stress concentrations in the competitive welded joints. Experiments with tensile, compressive and in-plane bending joint load were conducted on series of 45° and 90° X joint specimens in small-scale with CHS 60.3/4 brace members. Tensile test was conducted also on larger specimens of 45° X joint with CHS 219/6 brace members to understand differences in failure mode dominance at two different scales. Elastic stiffness, elastic load limit and ultimate load were analyzed from load-displacement behavior based on limited number of specimens tested, at least 3 nominally identical specimens in each series. Two major failure modes of wrapped composite joint, failure on primary bonded interface and cracking of composite material, accompanied by steel CHS yielding, were observed and quantified with help of 3D DIC results. Following conclusions are drawn:

1) In tensile, compressive and bending experiments the ultimate failure load of wrapped composite joints exceeds the yield resistance of the steel brace CHS. Clearly there is opportunity for optimization of composite wrap thickness and length.
2) Wrapped composite joints exhibit quasi-ductile failure. The gradual loss of secant stiffness during the inelastic stage is attributed to initiation and growth of partial debonding of the secondary bonded interface on the chord and development of debonding on the primary bonded interface on the brace.
3) The final failure of wrapped composite joints is due to full debonding on the brace and pull-out of the steel brace member from the composite wrap in tensile experiments in both small and medium scales. Partial debonding combined with cracking of the composite material is the governing failure mode in the bending experiment.
4) Wrapped composite joints in smaller scale have 30% to 56% larger joint stiffness, 18% to 44% larger elastic load limit and 3% to 83% larger ultimate load at failure compared to welded counterparts loaded in tension and bending.
5) Wrapped composite joints in smaller scale loaded in compression show 5% larger joint stiffness, 21% larger elastic load limit and 4% larger ultimate load than wrapped composite joints in tension. This is due to the direct contact between the brace and the chord member at the root of the joint.
6) Wrapped composite joints in larger scale (brace diameter 219 mm) show linear elastic behavior in axial tension up until a minimum of 1053 kN which is 82% higher than the characteristic resistance of the counterpart welded joints calculated according to EN 1993-1-8.
7) Wrapped composite joints show linear elastic behavior up until 52% to 64% of the ultimate load on braces in smaller-scale and larger-scale tensile or compressive joint experiments. In smaller-scale bending joint experiments inelastic behavior is initiated at 30% of the ultimate lateral load on the brace.

CRediT authorship contribution statement

Pei He: Investigation, Data curation, Writing – original draft preparation, Visualization, Formal analysis, Validation. **Marko Pavlovic:** Conceptualization, Methodology, Supervision, Commentary, Writing - reviewing and editing, Project administration, Funding acquisition, Resources.

Declaration of Competing Interest

The authors declare that they have no known competing financial interests or personal relationships that could have appeared to influence the work reported in this paper.

Acknowledgments

This research is supported by NWO (Netherlands Organization for Scientific Research) under Demonstrator project “Fatigue resistant Wrapped FRP joints of structural hollow sections”, proj. no. 16949. The first author would also like to express his gratitude for the financial support from China Scholarship Council (CSC) under grant number of 201806260242. The authors are grateful for the acknowledge provision and fabrication of the wrapped composite joints by Versteden b.v. and Ask Romein b.v. The authors are very grateful for the assistance of technicians from Steven Lab II of TU Delft.

References

[1] Wardenier J, Packer JA, Zhao XL, Van der Vegte GJ. Hollow sections in structural applications. Rotterdam, The Netherlands: Bouwen met staal; 2002.
[2] Vuong N, Quan M. Fatigue analysis of jacket support structure for offshore wind turbines. J Sci Technol Civil Eng (STCE) - HUCE. 2019;13(1):46–59.
[3] Siriwardane SC, Adasooriya ND, Pavlou D. Fatigue strength curve for tubular joints of offshore structures under dynamic loading. Dynamics 2021;1(1):125–33.
[4] Shabakhty Naser, Tabatabaei Seyed Saeid. Sensitivity of fatigue assessment for offshore jacket platform to different pile–soil–structure interaction models. Ships Offshore Struct 2021. https://doi.org/10.1080/17445302.2021.1979919.
[5] Nussbaumer A, Borges L, Davaine L. Fatigue design of steel and composite structures: Eurocode 3: Design of steel structures, part 1–9 fatigue; Eurocode 4: Design of composite steel and concrete structures. John Wiley & Sons; 2012.
[6] Jiao H, Zhao X-L. CFRP strengthened butt-welded very high strength (VHS) circular steel tubes. Thin-walled Struct 2004;42(7):963–78.
[7] Haedir J, Bambach MR, Zhao X-L, Grzebieta RH. Strength of circular hollow sections (CHS) tubular beams externally reinforced by carbon FRP sheets in pure bending. Thin-walled Struct 2009;47(10):1136–47.
[8] Lesani M, Bahaari MR, Shokrieh MM. Numerical investigation of FRP-strengthened tubular T-joints under axial compressive loads. Compos Struct 2013;100:71–8.
[9] Lesani M, Bahaari MR, Shokrieh MM. Experimental investigation of FRP-strengthened tubular T-joints under axial compressive loads. Constr Build Mater 2014;53:243–52.
[10] Lesani M, Bahaari MR, Shokrieh MM. FRP wrapping for the rehabilitation of Circular Hollow Section (CHS) tubular steel connections. Thin-Walled Struct 2015;90:216–34.
[11] Fu Y, Tong L. Experimental Study on Behavior of CFRP-Strengthened Circular Hollow Section Gap K-Joints. 6th International Conference on Advances in Experimental Structural Engineering, University of Illinois, Urbana-Champaign, United States, August 1-2. 2015.
[12] Fu Y, Tong L, He L, Zhao X-L. Experimental and numerical investigation on behavior of CFRP-strengthened circular hollow section gap K-joints. Thin-Walled Struct 2016;102:80–97.
[13] Pavlovic M, Veljkovic M, Bogers P. Method for making a virgin joint between two separate structural hollow sections, and such a virgin joint. 2021.
[14] Liatzouras M. Feasibility of non-welded CHS steel joints adhesively bonded by GFRP. Delft: Delft University of Technology; 2018. MSc thesis.
[15] Pavlovic M, Veljkovic M, Liatzouras M. Wrapped FRP Joints of Steel Hollow Sections. Eighth International Conference on THIN-WALLED STRUCTURES – ICTWS 2018, Lisbon, Portugal, July 24-27. 2018.
[16] He P, Pavlovic M. Feasibility of Wrapped FRP Circular Hollow Sections Joints. Proceedings of the 17th International Symposium on Tubular Structures, National University of Singapore, Singapore, December 9-12. 2019.
[17] Zhao X-L, Zhang L. State-of-the-art review on FRP strengthened steel structures. Eng Struct 2007;29(8):1808–23.
[18] Buyukozturk O, Gunes O, Karaca E. Progress on understanding debonding problems in reinforced concrete and steel members strengthened using FRP composites. Constr Build Mater 2004;18(1):9–19.
[19] Xia SH, Teng JG. Behaviour of FRP-to-steel bonded joints. In: Proceedings of the international symposium on bond behaviour of FRP in structures. International Institute for FRP in Construction; 2005. p. 419–26.
[20] Fawzia S, Al-Mahaidi R, Zhao X-L. Experimental and finite element analysis of a double strap joint between steel plates and normal modulus CFRP. Compos Struct 2006;75(1-4):156–62.
[21] Colombi P, Poggi C. Strengthening of tensile steel members and bolted joints using adhesively bonded CFRP plates. Constr Build Mater 2006;20(1-2):22–33.
[22] Deng J, Lee MMK. Behaviour under static loading of metallic beams reinforced with a bonded CFRP plate. Compos Struct 2007;78(2):232–42.
[23] Haghani R. Analysis of adhesive joints used to bond FRP laminates to steel members–A numerical and experimental study. Constr Build Mater 2010;24(11):2243–51.
[24] Kim SJ, Smith ST, Young B. Effect of surface preparation on the strength of FRP-to-mild steel and FRP-to-stainless steel joints. In: Advances in FRP Composites in Civil Engineering. Berlin, Heidelber: Springer; 2011. p. 869–72.

[25] Fawzia S, Zhao X-L, Al-Mahaidi R. Bond–slip models for double strap joints strengthened by CFRP. Compos Struct 2010;92(9):2137–45.
[26] Yu T, Fernando D, Teng JG, Zhao XL. Experimental study on CFRP-to-steel bonded interfaces. Compos B Eng 2012;43(5):2279–89.
[27] Al-Mosawe A, Al-Mahaidi R, Zhao X-L. Effect of CFRP properties, on the bond characteristics between steel and CFRP laminate under quasi-static loading. Constr Build Mater 2015;98:489–501.
[28] Li C, Ke L, He J, Chen Z, Jiao Y. Effects of mechanical properties of adhesive and CFRP on the bond behavior in CFRP-strengthened steel structures. Compos Struct 2019;211:163–74.
[29] Zhou H, Torres JP, Fernando D, Law A, Emberley R. The bond behaviour of CFRP-to-steel bonded joints with varying bond properties at elevated temperatures. Eng Struct 2019;183:1121–33.
[30] Zhou H, Fernando D, Torero JL, Torres JP, Maluk C, Emberley R. Bond Behavior of CFRP-to-Steel Bonded Joints at Mild Temperatures: Experimental Study. J Compos Constr 2020;24(6):04020070.
[31] Hu Bo, Li Y, Jiang Y-T, Tang H-Z. Bond behavior of hybrid FRP-to-steel joints. Compos Struct 2020;237:111936.
[32] International Standard Organization. ISO 14126:1999, Fibre-reinforced plastic composites — Determination of compressive properties in the in-plane direction. https://www.iso.org/standard/23638.html (accessed April 6, 2021).
[33] International Standard Organization. ISO 527-1:2019, Plastics — Determination of tensile properties — Part 1: General principles. https://www.iso.org/standard/75824.html (accessed April 6, 2021).
[34] International Standard Organization. ISO 14129:1997, Fibre-reinforced plastic composites — Determination of the in-plane shear stress/shear strain response, including the in-plane shear modulus and strength, by the plus or minus 45 degree tension test method. https://www.iso.org/standard/23641.html (accessed April 6, 2021).
[35] EN 1993-1-8, Eurocode 3: Design of steel structures, Part 1-8: Design of joints, CEN, Brussels, 2005.